nature communications

Article

https://doi.org/10.1038/s41467-026-68590-2

Multiple hydrogen bonding enables large-area doped phosphorescent glasses with robust stability and high-temperature afterglow

Received: 9 September 2025

Accepted: 12 January 2026

Published online: 17 January 2026

Check for updates

Chuanli Chen[1,6], Yuezhen Yang[2,3,6], Lutong Zhang[1], Wenbo Dai[1,4] ✉, Yunxiang Lei[1,4] ✉, Miaochang Liu[1], Huayue Wu[1], Xiaobo Huang[1] ✉ & Dongpeng Yan[5] ✉

Molecular room-temperature phosphorescence (RTP) materials with compact and ordered structures organized by intermolecular interactions have proven to be a newly-emerged strategy for high-performance luminescence. However, typical crystalline materials exhibit intrinsic brittleness and compromised optical transparency due to their highly ordered packing, thereby restricting their applicability in diverse functional systems. Herein, a universal non-conjugated molecule (1,2,3,4-butane tetracarboxylic acid) with abundant hydrogen-bonding positions is introduced as a host matrix for supramolecular glasses (SGs) through a convenient evaporation-induced self-assembly procedure. A series of SGs doped with aromatic anhydride derivatives is fabricated, exhibiting highly efficient ultralong phosphorescence with afterglow up to 40 s and quantum yields of 56.8%. Experimental and computational studies show that the multiple hydrogen bonds synergistically facilitate glass formation by stabilizing disordered structures while establishing a rigid molecular matrix, which effectively suppressed non-radiative decay of triplet excitons. The doped SGs demonstrate largely enhanced phosphorescent performance, including high temperature afterglow up to 200 °C and robust tolerance in various extreme environments compared with crystal counterparts. Particularly, a large-scale fabrication (25 cm × 25 cm) and shaping capability that is unattainable by traditional crystals. This work thus offers significant potential of these SGs for advanced displays and anti-counterfeiting applications.

Molecular room-temperature phosphorescent (RTP) or long-afterglow luminescent materials, characterized by long-lived triplet excitons, have garnered significant attention due to their tunable chemical structures, favorable biocompatibility, and adaptable properties[1–3]. Triplet excitons are generated either indirectly via intersystem crossing (ISC) from short-lived singlet excitons or directly through charge recombination, which exhibit characteristic photophysical characteristics including extended lifetimes, large Stokes shifts, and stimuli-responsive behavior[4,5]. To achieve high-performance RTP materials, the coordinated manipulation of ISC to generate triplet

A full list of affiliations appears at the end of the paper. ✉e-mail: wbdai@wzu.edu.cn; yunxianglei@wzu.edu.cn; xiaobhuang@wzu.edu.cn; yandp@bnu.edu.cn

excitons and suppression of non-radiative decay to stabilize these excited states are two critical factors[6–8]. Accordingly, multiple strategies, including heavy-atom effect[9,10], crystal engineering[11–13], polymerization[14–16], supramolecular assembly[17], host-guest doping[18–20] and so on, have been well developed for efficiently achieving ultralong RTP. These approaches collectively address critical challenges in exciton dynamics and material stability. Therein, multicomponent host-guest doping strategies have demonstrated significant potential for developing organic small-molecular RTP materials[21]. Rigid molecular host matrices with strong intermolecular interactions effectively suppress non-radiative transitions, thereby enhancing RTP performance[22]. Nevertheless, the reliance on highly ordered crystalline structures in current organic-doped RTP systems still hinders their processability and large-scale fabrication for practical applications[23].

Molecule-based glasses provide distinct advantages in overcoming the aforementioned limitations, offering high optical transparency and enhanced processability by suppressing crystallization while maintaining comparable mechanical rigidity[24]. Moreover, by incorporation of multiple non-covalent interaction networks, such as hydrogen bonding and van der Waals forces, molecular glasses can provide a stable and rigid molecular environment to protect triplet excitons from ambient oxygen[25–28]. Recently, biomolecules such as amino acid derivatives and peptides have been successfully assembled into RTP glass materials through self-assembly techniques[29–33]. Additionally, the metastable amorphous state facilitates uniform dispersion of dopants, making it an effective host matrix for developing high-efficiency photoactive materials[34–36]. However, the disordered molecular packing in glass systems is traditionally considered an inherent limitation for dopant efficiency and lifetime, as various thermal motions can quench RTP emission[37]. Therefore, it remains a significant challenge of the appropriate balance between enhancing RTP performance while preserving the inherent advantages of the glassy systems.

Structural design of monomeric building blocks plays a crucial role in the glass-forming ability of molecular systems[33,38,39]. A non-planar or irregular molecular geometry is typically required to prevent orderly molecular stacking[34]. Moreover, the presence of strong intermolecular interactions is also essential for restricting motions around any molecular axis, inherently resisting crystallization[27,40–42]. Based on this concept, herein, we constructed molecular doped glass systems with highly efficient, ultralong and robust RTP (Fig. 1a). In this work, star-shaped 1,2,3,4-butane tetracarboxylic acid (BTA), rich in hydrogen-bond donors, serves as the glass precursor and can be processed into bulk transparent glass via a convenient evaporation-induced self-assembly procedure[29,43]. A series of aromatic multi-anhydride derivatives (NFD, BFT, and TFH) is doped as RTP guests to construct the supramolecular glasses (SGs). These guests are selected

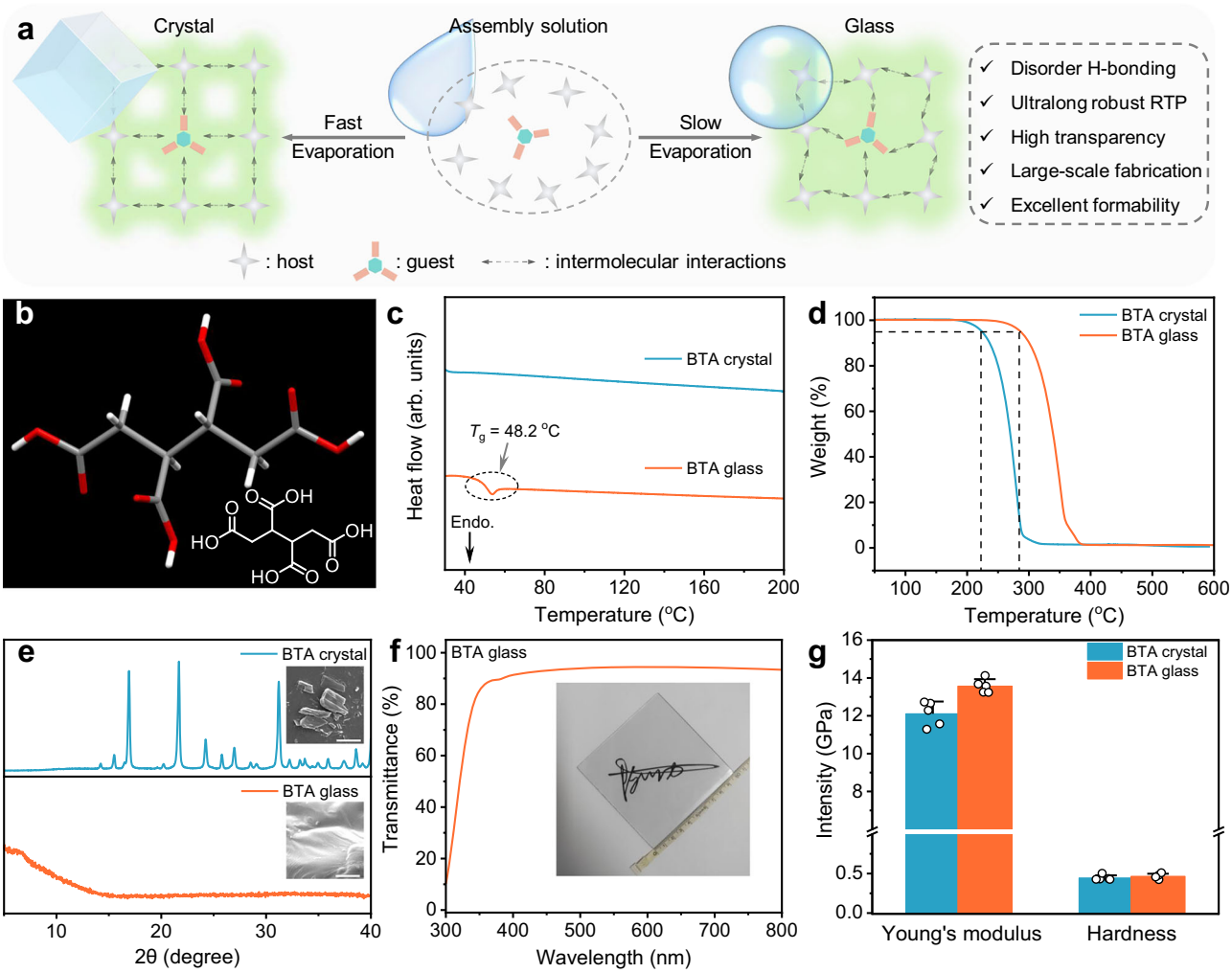

Fig. 1 | Design concept and material characterization. a Schematic diagram and the typical feature of molecule-based doped RTP glass system. **b** Molecular conformation and chemical structure of BTA. **c** DSC traces, **d** TGA curves, and **e** PXRD patterns and SEM pictures (insets) of BTA crystal and glass. **f** UV-Vis transmittance spectrum and photograph of BTA glass. **g** Young's modulus and hardness of BTA crystal and glass (Error bars represent standard deviation (SD). Data are presented as mean values ± SD from $n = 5$ independent measurements).

for their rigid aromatic cores and multiple carbonyl groups, which serve as hydrogen-bond acceptor sites to interact effectively with the BTA matrix and facilitate efficient ISC, significantly improving the phosphorescence performance. Experimental results and theoretical simulations demonstrate that multiple intermolecular hydrogen-bonding interactions stabilize the disordered structure, effectively suppressing molecular crystallization. Compared to the crystalline counterparts, the resulting SGs exhibit enhanced RTP performance and excellent stability, resisting luminescent quenching by oxygen, high temperature, and organic solvents. Furthermore, the hydrogen-bond networks endow excellent formability and thermoplastic properties, allowing the fabrication of large-scale transparent ultralong afterglow films and integrated multi-color luminescent bulk glass. This work thus demonstrates the significant potential of multiple disordered hydrogen-bonding strategies for fabricating SGs for advanced optical applications.

Results

Preparation and structural characterizations of the SGs

The pristine SG was prepared using star-shaped, non-planar BTA molecules as building blocks owing to its abundant interaction sites that can effectively stabilize the disordered packing and suppress crystallization (Fig. 1b). During the preparation of BTA-based glass (Supplementary Fig. 8), BTA powder was first dissolved in ethanol to form a highly concentrated solution. The solvent was then gradually removed at room temperature through evaporation, leading to a viscous state due to supramolecular assembly between BTA molecules. Prolonged drying led to complete solvent removal and the formation of a transparent and rigid BTA glass. In contrast, rapid evaporation at elevated temperature (78 °C) only led to the formation of white BTA crystals (Supplementary Fig. 8), and thus both the evaporation rate and temperature play important roles in the glass formation. The thermal properties of both BTA crystal and glass were first characterized by differential scanning calorimetry (DSC) and thermogravimetric analysis (TGA). The DSC curve reveals a distinct glass transition temperature (T_g) of 48.2 °C for BTA glass, indicating their high glass-forming ability above room temperature (Fig. 1c)[27]. Furthermore, repeated DSC heating cycles reveal that BTA glass undergoes a stable phase transformation (Supplementary Fig. 9). The amorphous state of BTA glass is also validated by powder X-ray diffraction (PXRD) and the scanning electron microscope images (Fig. 1e)[33]. Moreover, there is no change in molecular structure during the formation of the amorphous BTA glass (Supplementary Fig. 10). Subsequently, the optical and mechanical properties in both glassy and crystalline states were systematically investigated. BTA glass exhibits over 90% transmittance in the 400–800 nm range, comparable to that of inorganic glasses, supramolecular hydrogels, and polymeric plastics (Fig. 1f)[44]. In addition, compared to its crystalline counterpart, enhanced absorption and fluorescence emission were observed in its glass state (Supplementary Fig. 11), likely due to the formation of a denser hydrogen-bonding network promoted by molecular disorder packing, which facilitated tighter cluster formation[45]. Consequently, BTA glass demonstrates a higher decomposition temperature, indicating improved thermal stability (Fig. 1d). Furthermore, it exhibits increased Young's modulus and hardness, further reflecting the increased structural rigidity arising from strong intermolecular interactions (Fig. 1g and Supplementary Fig. 12)[33]. Therefore, BTA glass with a densely packed and rigid microenvironment can effectively suppress non-radiative decay of triplet excitons, making it a promising host matrix for constructing transparent phosphorescent SGs materials with high-performance ultralong afterglow.

Photophysical properties of BTA-based doped SGs materials

To construct efficient RTP systems, three phthalic anhydride derivatives (NFD, BFT, and TFH, Supplementary Fig. 1) featuring both n–π* transition-promoting capabilities and intermolecular interaction sites, were selected as guest molecules[46]. Among them, NFD and BFT are commercially available, while TFH was synthesized in a high yield and fully characterized by nuclear magnetic resonance (NMR) spectra and high-resolution mass spectrometry (Supplementary Figs. 2–5). All guests were purified via recrystallization, and their purity was confirmed by high-performance liquid chromatography (Supplementary Fig. 7). The preparation of doped SGs and crystalline systems followed a similar procedure to that of pristine BTA glass and crystal. It should be noted that all guests show high luminous efficiencies in both solution and solid state, revealing a dual-phase emission characteristic (Supplementary Fig. 13 and Supplementary Table 1). However, as shown in Supplementary Fig. 14, none inherent phosphorescent nature could be observed for all the host or guest molecules in the solid state. Therefore, RTP was only achieved via a host-guest doped system. The optimal weight ratio was identified as 0.1% by systematically doping varying amounts of guest TFH into the BTA matrix (Supplementary Fig. 15a).

We next systematically investigated the photophysical properties of these doped SGs and crystalline systems under ambient conditions using steady-state photoluminescence (PL) spectra, delayed emission spectra, and time-resolved decay profiles. As shown in Fig. 2a, f, all three doped glasses exhibit bright blue-cyan fluorescence (*ca.* 410 nm) along with RTP afterglow, with maximum phosphorescence peaks observed at *ca.* 540 nm, 518 nm, and 522 nm, respectively. Note that the RTP in the doping systems intrinsically originates from the guests, as evidenced by the consistency in phosphorescence spectra between the doping systems and dilute 2-methyltetrahydrofuran solutions at 77 K (Supplementary Fig. 16)[9]. Furthermore, PXRD patterns of the doped SGs show negligible changes after doping the guest (Fig. 2b), indicating that guest incorporation does not disrupt the amorphous glassy nature of the BTA matrix. Further analysis of phosphorescence decay curves at room temperature reveals phosphorescence lifetimes (τ_P) of 1.62, 2.82, and 3.80 s for NFD/BTA, BFT/BTA, and TFH/BTA, respectively (Fig. 2c), consistent with the fading afterglow observed in Fig. 2e. The longest afterglow persists for at least 40 s in the dark, and can be even observable for nearly 20 s under ambient daylight conditions (Supplementary Movie 1). RTP efficiencies (Φ_P) for NFD/BTA, BFT/BTA, and TFH/BTA reach 5.7%, 27.6%, and 56.8%, respectively (Fig. 2e and Supplementary Table 2). While achieving both high Φ_P and long τ_P in purely organic materials at room temperature remains intrinsically challenging, our system demonstrates a Φ_P of 56.8% and τ_P of 3.8 s under ambient conditions, which represents one of the best phosphorescent performances reported for purely organic RTP materials to date[47]. Additionally, the increase in the proportion of phosphorescence within the steady-state PL spectra is observed with the more anhydride units in the guest molecules (Fig. 2a). Both Φ_P and τ_P exhibit consistent trends (Fig. 2c, d, e). This behavior is likely attributed to the introduction of more lone-pair electrons, which significantly promote the ISC for generating triplet excitons. Moreover, the presence of more hydrogen-bonding sites facilitates the formation of denser hydrogen-bonded networks, effectively restricting molecular motions and ultimately leading to enhancing RTP emission[48].

Furthermore, the corresponding doped crystalline materials were also characterized. As illustrated in Supplementary Fig. 17, although the crystalline materials exhibit similar emission wavelengths to those of the doped SGs systems in the steady-state PL spectra, the contribution of phosphorescence is significantly reduced. This results in notably lower Φ_P and τ_P for the crystalline materials compared to their glass counterparts (Fig. 2d, e and Supplementary Table 2). To gain deeper insight into the phosphorescent behavior of these doped materials, we calculated the ISC rate (k_{ISC}) and non-radiative decay rate of phosphorescence (k_{nr}^P)[8]. As shown in Fig. 2e and Supplementary Table 2, SGs-based systems exhibit higher k_{ISC} and significantly lower k_{nr}^P compared to their crystalline systems. These results demonstrate

https://doi.org/10.1038/s41467-026-68590-2

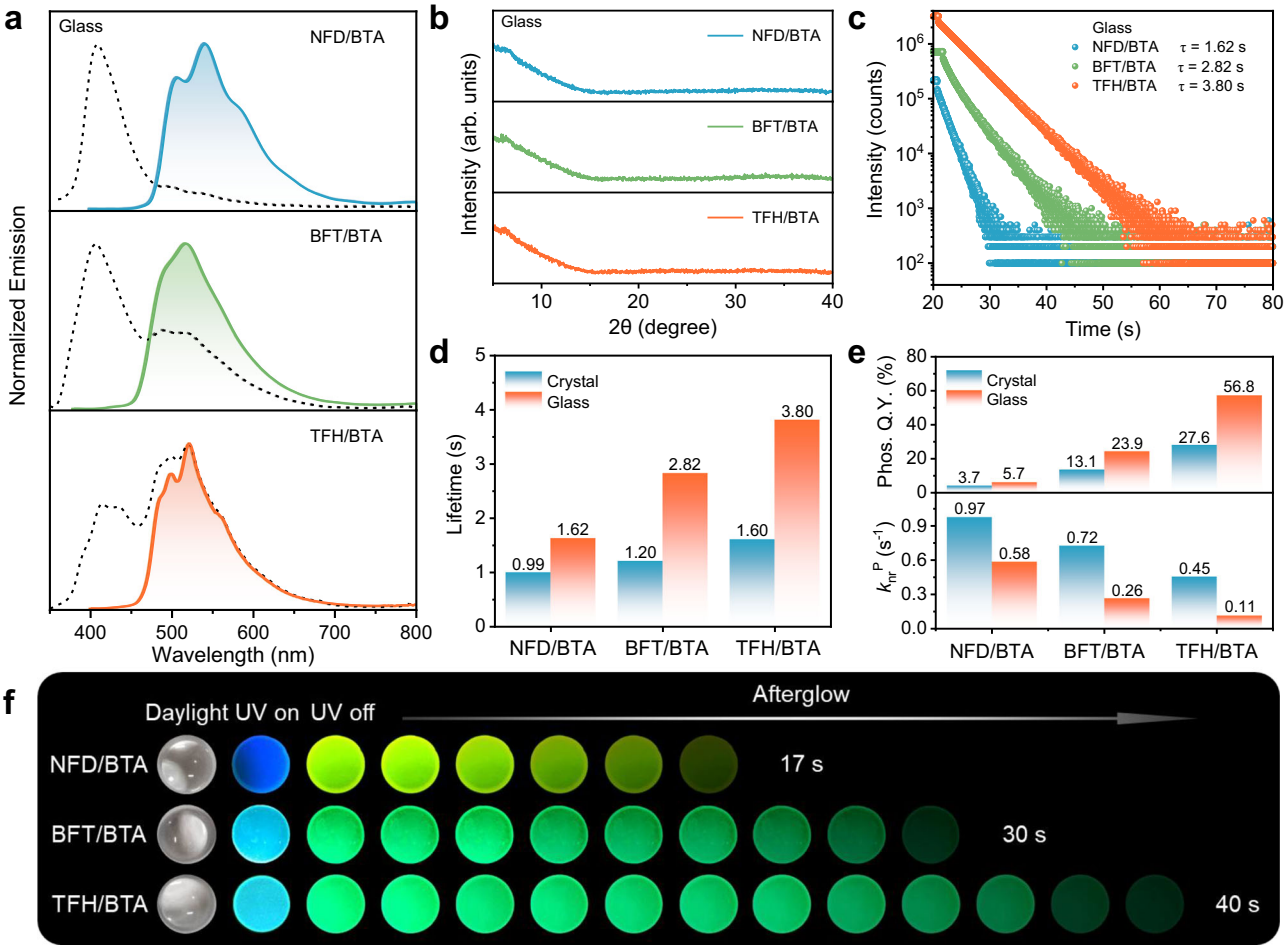

Fig. 2 | Photophysical properties of BTA-based doped materials under ambient conditions. a Normalized steady-state PL (dash line) and delayed (solid line, delayed time: 50 μs) emission spectra, **b** PXRD patterns, and **c** phosphorescence decay curves of BTA-based doped glass materials at room temperature. **d** Lifetime histograms, and **e** absolute phosphorescence quantum yields (Phos. Q.Y., top) and non-radiative decay rates (k_{nr}^P, bottom) histograms of BTA-based doped crystal (blue area) and glass (red area) materials, respectively (Note: a bar chart column represents a single measurement). **f** Photographs of BTA-based doped glass materials under daylight, 365 nm UV light on and off.

that the glass matrix effectively promotes the ISC process of the guest molecules while suppressing non-radiative decay, ultimately generating highly efficient and long-lived RTP. Evidently, BTA glass serves as an excellent matrix for constructing high-performance phosphorescent materials.

Mechanism of the BTA-based efficient phosphorescence glasses

To gain deeper insight into the mechanism behind the efficient RTP of BTA-based doped SGs, the molecular packing of BTA glass was obtained through molecular dynamics (MD) simulations[39]. The results indicate that BTA glass exhibits long-range disordered molecular arrangements (Fig. 3a). It is found that the molecular structure of BTA in the amorphous glass state is more distorted, enabling the formation of a random and irregular hydrogen-bonding network through carboxyl groups interacting with surrounding BTA molecules (Fig. 3a and Supplementary Fig. 19). This is further confirmed by Fourier-transform infrared (FT-IR) spectroscopy (Supplementary Fig. 20), where BTA glass displays a broad, unstructured O–H stretching vibration peak between 2500 and 3500 cm^{-1}, suggesting the existence of multiple disorder intra- and intermolecular hydrogen bonding within such glass[49]. This irregularity may suppress crystallization by restricting molecular diffusion, thereby favoring the formation of disordered glass[33]. Furthermore, as shown in Fig. 3a, typical molecular clusters within the BTA glass contain multiple strong hydrogen bonds, including C–H···O (2.281–2.587 Å) and O–H···O (2.052–2.607 Å). This robust hydrogen bonding network provides BTA glass with high mechanical strength and thermal stability. Moreover, compared to the crystalline materials, which exhibit more pronounced quenching effects in air, the delayed emission spectra and phosphorescence decay of the TFH/BTA glass show no obvious changes under various atmospheric conditions (Supplementary Figs. 21 and 22). This further demonstrates the excellent role of the disordered hydrogen bonding network in inhibiting non-radiative decay. Then, the independent gradient model based on Hirshfeld partition of molecular density (IGMH) was employed to investigate the non-covalent interactions within BTA glass[50,51]. Various interactions between molecular clusters are visualized in Fig. 3b. The IGMH map clearly shows multiple strong O–H···O hydrogen bond interactions (represented by blue isosurfaces in the central area) between BTA molecules. Additionally, the broad green isosurfaces reveal the existence of multiple C–H···O hydrogen bonds and strong van der Waals interactions. Overall, the MD simulation results indicate that the BTA-based SG forms more and stronger disordered hydrogen bonds, which stabilize its conformation and contribute to the excellent phosphorescent performance.

To further investigate the role of disordered hydrogen bonds in suppressing non-radiative transitions within BTA glass, we selected non-aromatic acids succinic acid (BDA) and 1,2,3-propanetricarboxylic acid (PTA), which have similar molecular structures to BTA but feature different carboxyl groups, as the reference hosts (Fig. 3c). Under ambient conditions, both TFH/BDA and TFH/PTA crystalline materials

https://doi.org/10.1038/s41467-026-68590-2

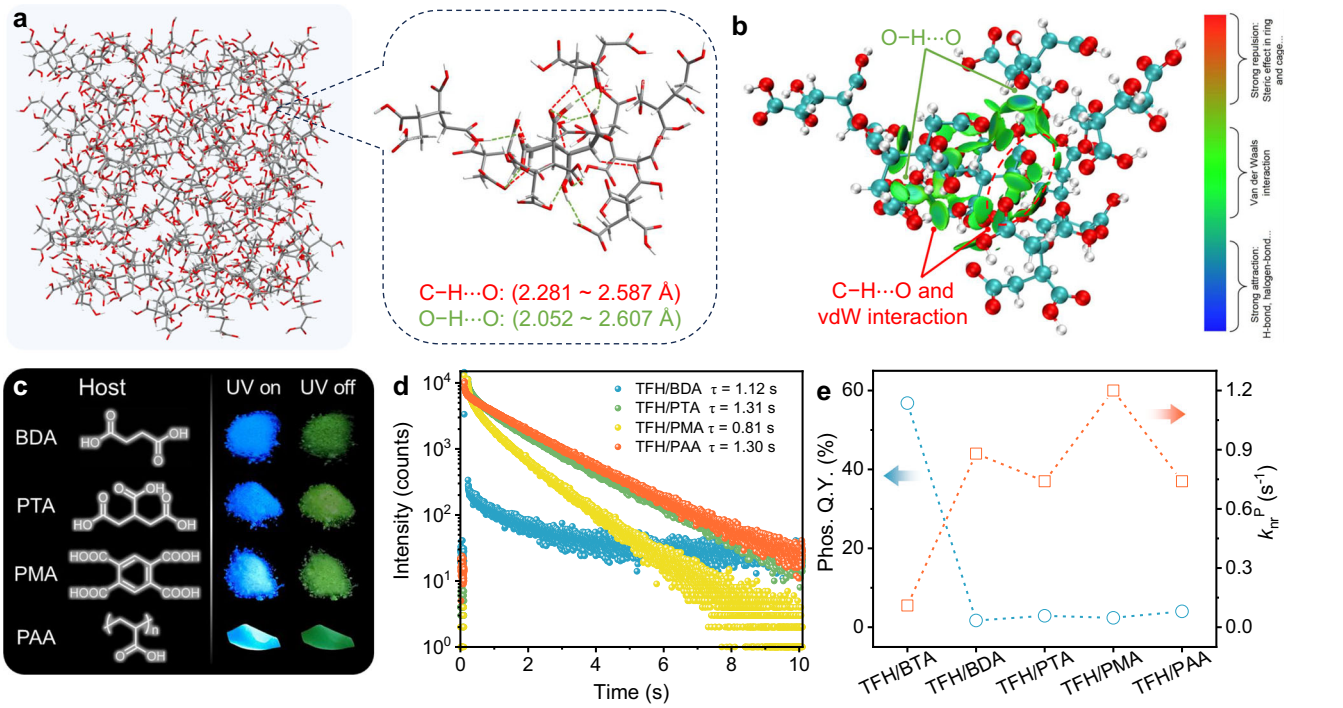

Fig. 3 | Mechanistic investigations of BTA-based doped SGs under ambient conditions. a Molecular packing mode of BTA amorphous glass obtained through molecular dynamics simulations, and the hydrogen-bonding interactions within typical molecular clusters that represent the local arrangement inside the BTA glass. **b** IGMH analysis of the non-covalent interactions in BTA glass (the isosurface corresponds to δg^{inter} of 0.005 a.u., and the color bar range is from −0.05 to 0.05 a.u.). Strong hydrogen bonds and van der Waals interactions were demonstrated within the BTA molecules. **c** Chemical structures of reference hosts and photographs of the corresponding doped materials under 365 nm UV light on and off. **d** Phosphorescence decay curves, and **e** variation tendency of phosphorescence quantum yields (Phos. Q.Y.) and non-radiative decay rates (k_{nr}^P) of the doped materials under ambient conditions.

exhibit RTP with lifetimes of 1.12 s and 1.31 s, respectively (Fig. 3d and Supplementary Fig. 23). However, due to reduced hydrogen bond positions in the host molecules, the formation of a continuous, multidimensional hydrogen bond network to suppress non-radiative transitions is hindered, resulting in significantly lower Φ_P of only 1.12 and 1.31% (Fig. 3d, Supplementary Figs. 24, 25 and Table 3). Furthermore, we examined the effect of suppressing k_{nr}^P in other typical host-guest systems, including the aromatic acid TFH/PMA (1,2,4,5-benzenetetracarboxylic acid) with the same carboxyl group and the polymer TFH/PAA (polyacrylic acid) with strong hydrogen bonding interactions (Fig. 3c)[52]. Although these doped materials also exhibit RTP emission, their low Φ_P can similarly be attributed to high k_{nr}^P (Fig. 3e). These results highlight the critical role of disordered hydrogen bonds in BTA SGs in suppressing non-radiative decay, ultimately leading to efficient phosphorescence in the BTA-based doped SGs.

Universality and high stability of BTA-based doped SGs

To evaluate the universality of the BTA matrix in constructing high-performance RTP SGs, we examined three additional anhydride derivatives (BPA, NID, and NIT, Supplementary Fig. 1) as guest molecules to prepare the corresponding doped glass materials. Consistently, the phosphors embedded in the disordered BTA glass matrix exhibited efficient RTP. The long-lived phosphorescence emission with peaks at 484, 548, and 606 nm (Fig. 4a), with corresponding lifetimes of 0.11, 0.47, and 0.07 s, respectively (Fig. 4b). These delayed spectra closely matched the phosphorescence spectra of the guest molecules at low temperature (Supplementary Fig. 28). The CIE coordinates of the persistent emissions fell within the blue, green, yellow, and red regions (Fig. 4c), demonstrating the capability of this amorphous organic glass system to generate full-color afterglow.

Notably, the BTA-based doped glass exhibits exceptional high-temperature tolerance. As shown in Fig. 4d and Supplementary Fig. 29a, the fluorescence peak at ~410 nm remains stable in the low-temperature region (approximately 20–100 °C) before decreasing at elevated temperatures, while the phosphorescence intensity of TFH/BTA gradually decreases at 522 nm as the temperature rises from 20 °C to 200 °C. As a result, the range of luminous colors can be greatly adjusted from cyan to blue (Supplementary Fig. 29b). A similar trend is observed for the phosphorescence lifetime (Supplementary Fig. 30). The temperature-dependent FT-IR spectra of the TFH/BTA-doped glass were also recorded (Supplementary Fig. 31). All of the vibration signals significantly increase in intensity and gradually broaden as the temperature increases. The diminished emission and shortened lifetime at elevated temperatures are attributed to the weakening of intermolecular hydrogen bonding interactions in the doped glass, which leads to the enhanced non-radiative decay from both singlet and triplet excitons[53]. Even at 200 °C, TFH/BTA glass retains a sufficient phosphorescent signal and visible afterglow (Fig. 4d and Supplementary Figs. 30, 32, 200 °C, τ_P = 0.33 s). It should be noted that efficient phosphorescence emission from purely organic materials at such elevated temperatures has rarely been reported (Supplementary Table 4)[54]. Additionally, the TFH/BTA-doped glass demonstrates exceptional long-term thermal stability and reversibility that can undergo many heat/cool cycles (Supplementary Figs. 33 and 34). It also exhibits excellent photostability, retaining its performance under continuous UV irradiation for hours (Supplementary Fig. 35). This exceptional performance is attributed to the multiple disordered hydrogen-bonding networks within the BTA glass matrix, which create a robust and rigid environment that suppresses non-radiative decay, thereby enabling effective afterglow emission even under extreme thermal conditions. Moreover, the doped glass exhibits high stability, maintaining its amorphous state for over three months under ambient conditions without any observable crystallization (Supplementary Fig. 36). Notably, the TFH/BTA doped glass retains robust RTP

https://doi.org/10.1038/s41467-026-68590-2

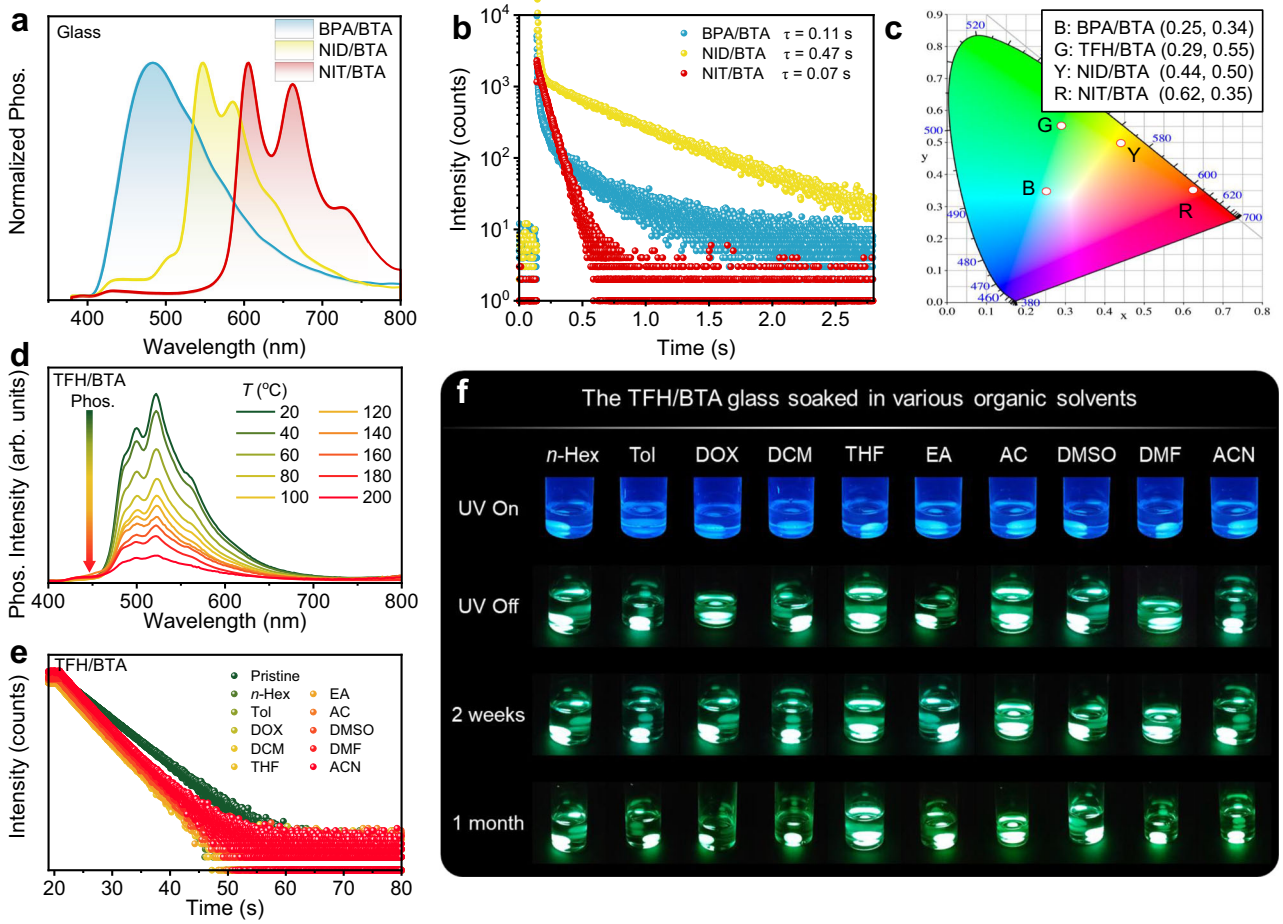

Fig. 4 | Universality and stability of BTA-based doped glasses. a Normalized phosphorescence (Phos., delayed time: 50 μs) emission spectra, **b** Phosphorescence decay curves, and **c** CIE coordinates of BTA-based doped glass materials. **d** Phosphorescence (Phos., delayed time: 50 μs) emission spectra of the TFH/BTA glass at different temperature. **e** Phosphorescence decay curves of TFH/BTA glass after soaking in different solvents for 1 month. **f** Photographs of TFH/BTA glass after soaking in different solvents for 2 weeks and 1 month. *n*-Hex, Tol, DOX, DCM, THF, EA, AC, DMSO, DMF, and ACN represent *n*-hexane, toluene, 1,4-dioxane, dichloromethane, tetrahydrofuran, ethyl acetate, acetone, dimethyl sulfoxide, *N*,*N*′-dimethylformamide, and acetonitrile, respectively.

performance even after prolonged soaking in a variety of solvents covering a wide polarity range, with a minimal decrease in RTP lifetime (Fig. 4e, f, and Supplementary Fig. 37). These results fully demonstrate the universality of our doped glass systems. The multiple disordered hydrogen-bonding network within the BTA matrix effectively prevents the quenching of the triplet state of doped phosphors, enabling the resulting phosphorescent glass to exhibit both high RTP performance and excellent stability, which are promising for practical applications.

Applications of BTA-based doped glass

Benefiting from the excellent solution-processable glass-forming ability and highly efficient persistent afterglow, the feasibility of BTA-based doped glass was further demonstrated in large-scale fabrication, thermoplastic processing, and advanced information-encryption display technologies. As shown in Fig. 5a and Supplementary Fig. 38a, a viscous host-guest doped solution was uniformly coated onto a 25 cm × 25 cm quartz substrate. After solvent evaporation, a large-area, uniform, and transparent afterglow glass was obtained. The uniformity of phosphorescence performance across the panel was confirmed by measuring the intensity and lifetime at different regions of the panel (Supplementary Fig. 38). The high optical transparency and scalable fabrication capability of the afterglow glass highlight its potential for optical device applications. For example, in dark conditions, the 25 cm × 25 cm afterglow panel can serve as a lighting device, providing illumination for emergency evacuation maps. Conventional inorganic glasses with high T_g typically require harsh processing conditions (such as elevated temperatures) and are difficult to shape. These limitations hinder their integration into modern manufacturing techniques, such as 3D manufacturing[55]. In contrast, the BTA-based glass exhibits a relatively low T_g of 48.2 °C and transitions to a rubbery state above this temperature (Fig. 1c), indicating that it can be thermoplastically processed when the temperature is slightly above 50°C, thus enabling low-temperature manufacturing. Therefore, bulk afterglow glass in arbitrary 3D shapes can be fabricated using specific molds, without distortion and crystallization tendency during processing (Fig. 5b, top). More interestingly, under mild thermal processing, the doped glasses with different shapes can be easily combined to an integrated bulk glass exhibiting multicolor afterglow (Fig. 5b, bottom, and Supplementary Movies 2 and 3). Moreover, the ultralong afterglow emission of BTA-based glasses can be combined with electrical excitation for information-encryption displays. By evaporating solutions containing different guest dopants, BTA-based glasses are coated onto a commercial 365 nm LED array[14]. As shown in Fig. 5c, upon powering the LEDs, a bright blue-cyan fluorescence is observed. Due to the distinct afterglow decay times of the doped glasses, switching off the direct current led to the emergence of different numerical patterns with varying durations. These results highlight the potential of the high-transparency, large-scale processable afterglow glass for advanced optical device applications.

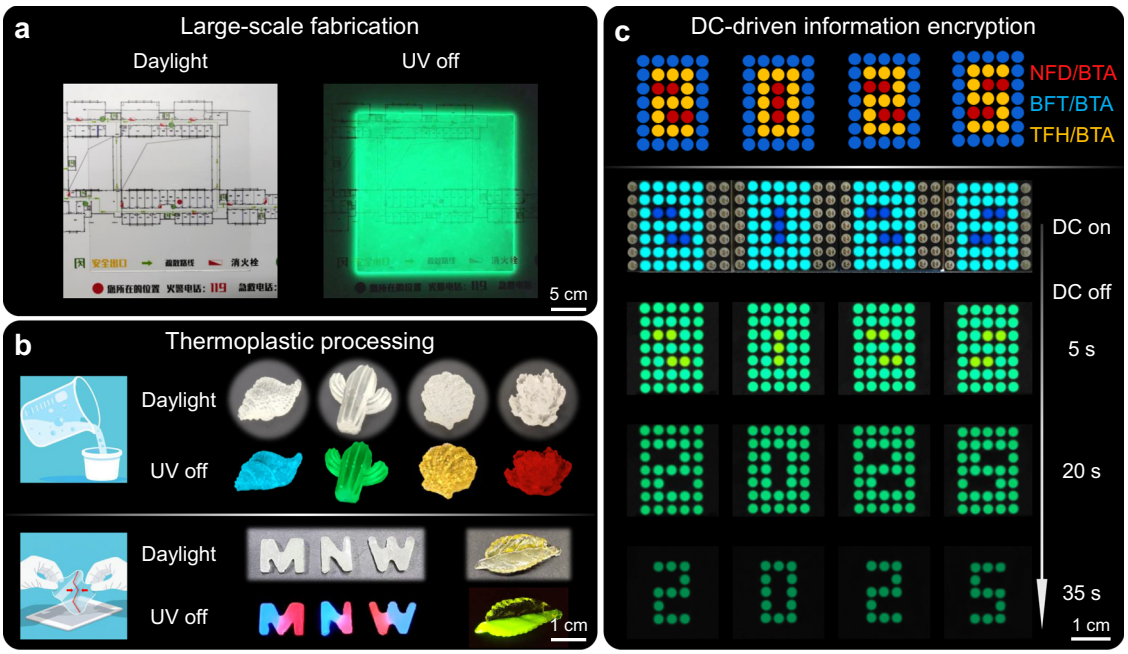

Fig. 5 | Demonstration of large-scale fabrication and thermoplastic processing of BTA-based doped glass for the potential application. a Photographs of the fabricated large-scale TFH/BTA glass afterglow panel under daylight and 365 nm UV light off (scale bar = 5 cm). Note that the afterglow panel can light up the map of the emergency evacuation route. **b** Photographs of thermoplastic processability of BTA-based doped glass under daylight and 365 nm UV light off (scale bar = 1 cm). **c** Digit information-encryption display using BTA-based doped glass under direct current (DC) switched on and off, with different time passing from top to down (scale bar = 1 cm).

Discussion

In summary, we have developed an approach for fabricating efficient organic RTP glasses through the integration of multiple disordered hydrogen bonds. By leveraging the non-planar, multi-carboxylic acid BTA as a universal host, we demonstrate that long-range disordered yet locally dense hydrogen-bond networks synergistically suppress non-radiative decay pathways while enabling exceptional glass-forming capability. This approach yields excellent RTP yields up to 56.8% and ultralong afterglows exceeding 40 s, which outperform the as-reported RTP glass family. The adaptability of the BTA-based system further extends to the formation of multi-color afterglow materials. The glass system also demonstrates stability under various extreme conditions, maintaining visible afterglow even at elevated temperatures (up to 200 °C, $\tau_P = 0.33$ s). Moreover, the BTA-based doped glass exhibits incomparable formability compared to its crystalline counterparts, enabling the production of large-scale and transparent panels, and multi-color afterglow bulk glasses. Therefore, this work offers a promising pathway for the fabrication of highly efficient RTP glass using a multiple disordered hydrogen-bonding strategy, with promising applications in advanced optical display and information encryption.

Methods

Materials and characterization

All the host and guest molecules (except TFH) were commercially purchased. All guest molecules were purified by column chromatography twice, followed by recrystallization. 2,3-Naphthalenedicarboxylic Anhydride (99%), 3,3′,4,4′-Biphenyltetracarboxylic dianhydride (98%), 4,4′-(4,4′-isopropylidenediphenoxy)bis-(phthalic anhydride) (99%), 1,8-Naphthalic anhydride (99%), 1,4,5,8-Naphthalenetetracarboxylic dianhydride (99%), Hexakis(bromomethyl)benzene (98%), Dimethyl 2-butynedioate (98%), NaI (99%), MnO_2 (98%), KOH (99%), Thionyl chloride (99%), Succinic acid (99%), Tricarballylic acid (99%), Pyromellitic acid (99%), Poly(acrylic acid) (M_w = 45000 g/mol), *N*,*N*-Dimethylformamide (99.99%), Toluene (99.99%), Tetrahydrofuran (99.99%) were purchased from Aladdin, Bide Pharmatech Ltd, and Energy Chemical.

^{1}H and ^{13}C NMR spectra were carried out by a Bruker ARX400 spectrometer with DMSO-d_6 as the solvent. UV-vis absorption spectra were measured by Persee TU-1901. Mass spectra were performed by using Finnigan BIFLEX III mass spectroscopy. The thermogravimetric curves and heat flow curves of all the samples were measured using a TGA instrument (ZCT-A) and a DSC 300 Calirls. Scanning electron microscopy (SEM 3100, CIQTEK Ltd.) was used to observe the surface morphology of the glass. PXRD data were measured by Smartlab SE (Rigaku Corporation). Fourier transform infrared (FT-IR) spectra were acquired using a Vertex 70 infrared spectrophotometer (Bruker, Germany). Temperature-dependent FT-IR spectra were recorded by a Nicolet 6700 instrument (Thermo Scientific) and a Linkam THMS600 in the transmission mode. Steady PL spectra and delayed emission spectra of host-guest doped materials were measured by using Nanolog FL3-2iHR (Horiba Jobin Yvon). The emission quantum yields were collected by using a FluoroMax-4 (Horiba Jobin Yvon) fluorimeter equipped with an integrated sphere. By peak-differentiation-imitating analysis, the phosphorescent and fluorescent quantum yields from the absolute total PL quantum yields can be figured out from their integrated area ratios identified from the steady-state PL spectrum. PL time-resolved decays were measured with a DeltaFlex ultrafast lifetime spectrofluorometer.

Computational details

The amorphous structure of BTA was constructed by the Amorphous Cell module by the Universal force field in the Material Studio 2017. By the Forcite module, a standard procedure including energy minimization, and a 20 ns *NPT* ensemble simulation (P = 1 atm and T = 300 K), as well as a 20 ns *NVT* ensemble simulation (T = 300 K), was performed to equilibrate the structure and obtain the stable film conformation. After the equilibration, a 20 ns production run in *NVT* ensemble (T = 300 K) was performed to collect data. Besides, a representative conformation of the equilibrated system was chosen

for further calculations. IGMH analysis of weak interaction based on amorphous structure was conducted by using Multiwfn[56,57]. The corresponding structure and IGM isosurfaces were generated using VMD 1.9.3 software[58].

Preparation of glass and crystalline powder

First, 1 g of BTA powder is dissolved in 10 ml of ethanol and stirred under a nitrogen atmosphere at 350 K for 6 h. The resulting transparent, viscous liquid is then thermally dropped onto a 1.5 cm × 1.5 cm quartz substrate. The sample is heated at 313 K for 12 h and at 373 K for 4 h, yielding a transparent glass and a white crystalline powder, respectively.

Preparation of afterglow glass and crystalline powder

Firstly, two solutions were prepared: one containing organic phosphors dissolved in ethanol at a concentration of 10 mg/mL, and the other a homogeneous alcohol solution of BTA, prepared by dissolving 1 g of BTA in 10 mL of distilled ethanol and heating at 350 K for 6 h. As an example, 1.0 wt% of the phosphor solution (1 mL) was added to the BTA solution (10 mL) and mixed at 350 K for 6 h. The resulting mixture was then dropped onto a 1.5 cm × 1.5 cm quartz wafer, which was vacuum-dried at 313 K for 12 h and at 373 K for 4 h, yielding a transparent glass and a white crystalline powder, respectively.

Preparation of bulk afterglow glass with various shapes and a large-area afterglow panel

The mixed solution was prepared following the steps outlined above. It was then poured into a prepared silicone mold, and air bubbles were removed by gentle shaking. The mold was placed in a vacuum oven at 313 K for 24 h. Finally, bulk afterglow glass with various shapes was obtained by demolding. For the preparation of large-area afterglow panels, the mixed solution was prepared following the steps outlined above. The resulting solution was poured into a quartz mold (2 cm deep, 25 cm × 25 cm) and vacuum-dried at 313 K for 24 h. Finally, a large-area afterglow glass panel was obtained.

Preparation of integrated bulk glass

Two distinct phosphorescent glass objects were fabricated using the afterglow glass preparation method. Upon heating the materials to 330 K, both glass types exhibited a certain degree of viscosity and softness, allowing them to be plastically fused into thermoplastic materials.

Data availability

All the data generated in this study are provided in the article and the Supplementary Information, or are also available from the corresponding authors upon request. The X-ray crystallographic coordinates for structures reported in this study are downloaded from the Cambridge Crystallographic Data Centre (CCDC), under deposition numbers 726433 (BTA), 154423 (BDA) and 233347 (PTA). These data can be obtained free of charge from The Cambridge Crystallographic Data Centre via www.ccdc.cam.ac.uk/data_request/cif. Source data are provided with this paper.

References

1. Zhao, W., He, Z. & Tang, B. Z. Room-temperature phosphorescence from organic aggregates. *Nat. Rev. Mater.* **5**, 869–885 (2020).
2. Kenry, Chen, C. & Liu, B. Enhancing the performance of pure organic room-temperature phosphorescent luminophores. *Nat. Commun.* **10**, 2111 (2019).
3. Dai, W. et al. Recent progress in ion-regulated organic room-temperature phosphorescence. *Chem. Sci.* **15**, 4222–4237 (2024).
4. Lei, Y. et al. Stimulus-responsive organic phosphorescence materials based on small molecular host-guest doped systems. *J. Phys. Chem. Lett.* **14**, 1794–1807 (2023).
5. Yin, G. et al. Targeting compact and ordered emitters by supramolecular dynamic interactions for high-performance organic ambient phosphorescence. *Adv. Mater.* **36**, e2311347 (2024).
6. Shi, H., Yao, W., Ye, W., Ma, H., Huang, W. & An, Z. Ultralong organic phosphorescence: from material design to applications. *Acc. Chem. Res.* **55**, 3445–3459 (2022).
7. Cai, S., Yao, X., Ma, H., Shi, H. & An, Z. Manipulating intermolecular interactions for ultralong organic phosphorescence. *Aggregate* **4**, e320 (2023).
8. Ye, W. et al. Confining isolated chromophores for highly efficient blue phosphorescence. *Nat. Mater.* **20**, 1539–1544 (2021).
9. Dai, W. et al. Halogen bonding: a new platform for achieving multi-stimuli-responsive persistent phosphorescence. *Angew. Chem. Int. Ed.* **61**, e202200236 (2022).
10. Hamzehpoor, E., Ruchlin, C., Tao, Y., Liu, C. H., Titi, H. M. & Perepichka, D. F. Efficient room-temperature phosphorescence of covalent organic frameworks through covalent halogen doping. *Nat. Chem.* **15**, 83–90 (2023).
11. Singh, M. et al. Achieving high-temperature phosphorescence by organic cocrystal engineering. *Angew. Chem. Int. Ed.* **63**, e202319694 (2024).
12. Ye, W. et al. High-performance circularly polarized phosphorescence by confining isolated chromophores with chiral counterions. *Adv. Mater.* **36**, e2410073 (2024).
13. Ruchlin C. et al. Divergent synthesis and crystal engineering of room-temperature phosphorescent carbonyl-bridged triphenylamines. *Angew. Chem. Int. Ed.* **64**, e202512446 (2025).
14. Zhang, X. et al. Multicolor hyperafterglow from isolated fluorescence chromophores. *Nat. Commun.* **14**, 475 (2023).
15. Gan, N. et al. Stretchable phosphorescent polymers by multiphase engineering. *Nat. Commun.* **15**, 4113 (2024).
16. Chen, Q. et al. Long lifetimes white afterglow in slightly crosslinked polymer systems. *Nat. Commun.* **15**, 2947 (2024).
17. He, Z., Song, J., Li, C., Huang, Z., Liu, W. & Ma, X. High-performance organic ultralong room temperature phosphorescence based on biomass macrocycle. *Adv. Mater.* **37**, e2418506 (2025).
18. Xu, S. et al. Design of highly efficient deep-blue organic afterglow through guest sensitization and matrices rigidification. *Nat. Commun.* **11**, 4802 (2020).
19. Zhang, Y. et al. Ultraviolet irradiation-responsive dynamic ultralong organic phosphorescence in polymeric systems. *Nat. Commun.* **12**, 2297 (2021).
20. Chen, K. et al. Twofold rigidity activates ultralong organic high-temperature phosphorescence. *Nat. Commun.* **15**, 1269 (2024).
21. Yin Z., Wu Z., Liu B. Recent advances in impurity-induced room-temperature phosphorescence. *Adv. Mater.* **37**, e2506549 (2025).
22. Li K., et al. "Strong Assisting Weak" effect for long-lived room temperature phosphorescence in host–guest-doped systems. *Angew. Chem. Int. Ed.* **64**, e202508587 (2025).
23. Xue, Y., Xie, Z., Yin, Z., Xu, Y. & Liu, B. Full-color processible afterglow organic small molecular glass. *Nat. Commun.* **16**, 4526 (2025).
24. Nie, F. & Yan, D. Supramolecular glass: a new platform for ultralong phosphorescence. *Sci. China Mater.* **67**, 3531–3536 (2024).
25. Nie, F. & Yan, D. Macroscopic assembly of chiral hydrogen-bonded metal-free supramolecular glasses for enhanced color-tunable ultralong room temperature phosphorescence. *Angew. Chem. Int. Ed.* **62**, e202302751 (2023).
26. Nie, F. & Yan, D. Zero-dimensional halide hybrid bulk glass exhibiting reversible photochromic ultralong phosphorescence. *Nat. Commun.* **15**, 5519 (2024).
27. Zhang, M. et al. Dynamic organic phosphorescence glass by rigid-soft coupling. *Angew. Chem. Int. Ed.* **64**, e202415250 (2024).
28. Wang, M. et al. Solvent-free processing of lignin into robust room temperature phosphorescent materials. *Nat. Commun.* **16**, 2455 (2025).

29. Nie, F., Wang, K. Z. & Yan, D. Supramolecular glasses with color-tunable circularly polarized afterglow through evaporation-induced self-assembly of chiral metal-organic complexes. *Nat. Commun.* **14**, 1654 (2023).
30. Nie, F. & Yan, D. Bio-sourced flexible supramolecular glasses for dynamic and full-color phosphorescence. *Nat. Commun.* **15**, 9491 (2024).
31. Li, X., Yang, Y., Zhao, Z., Bai, S., Li, Q. & Li, J. General and versatile nanoarchitectonics for amino acid-based glasses via co-assembly of organic counterions. *Angew. Chem. Int. Ed.* **64**, e202422272 (2024).
32. Baker, O'Donnell, B. C., Priya, A. D., Hyder, M., German, I. M. & Hayes, W. A supramolecular glass made from a low molecular weight amino acid derivative. *Eur. Polym. J.* **162**, 110889 (2022).
33. Yuan, C., Fan, W., Zhou, P., Xing, R., Cao, S. & Yan, X. High-entropy non-covalent cyclic peptide glass. *Nat. Nanotechnol.* **19**, 1840–1848 (2024).
34. De Silva, A., Felix, N. M. & Ober, C. K. Molecular glass resists as high-resolution patterning materials. *Adv. Mater.* **20**, 3355–3361 (2008).
35. Cai, C., Wu, S., Zhang, Y., Li, F., Tan, Z. & Dong, S. Bulk transparent supramolecular glass enabled by host-guest molecular recognition. *Nat. Commun.* **15**, 3929 (2024).
36. Hou X. et al. The formation of a supramolecular rigid glass based on a transparent deep eutectic. *Adv. Mater.* **37**, e06637 (2025).
37. Cheng, A. et al. Disorder-Enhanced Charge-Transfer-Mediated Room-Temperature Phosphorescence in Polymer Media. *Angew. Chem. Int. Ed.* **62**, e202312627 (2023).
38. Finkelstein-Zuta, G. et al. A self-healing multispectral transparent adhesive peptide glass. *Nature* **630**, 368–374 (2024).
39. Xing, R., Yuan, C., Fan, W., Ren, X. & Yan, X. Biomolecular Glass with Amino Acid and Peptide Nanoarchitectonics. *Sci. Adv.* **9**, eadd8105 (2023).
40. Zhou, B., Qi, Z. & Yan, D. Highly Efficient and Direct Ultralong All-Phosphorescence from Metal–Organic Framework Photonic Glasses. *Angew. Chem. Int. Ed.* **61**, e202208735 (2022).
41. Xu, Z. et al. Supercooled Liquids with Dynamic Room Temperature Phosphorescence Using Terminal Hydroxyl Engineering. *Angew. Chem. Int. Ed.* **62**, e202301564 (2023).
42. Gu, S., Wu, Q. & Wu, J. Ultralong room temperature phosphorescence with multicolor afterglow achieved in a harsh polymeric viscous flow state. *Mater. Horiz.* **11**, 5692–5700 (2024).
43. Nie, F. & Yan, D. Molecular Glass from Solution Self-Assembly. *Acc. Chem. Res.* **58**, 3010–3020 (2025).
44. Zhang, Y. et al. Supramolecular control over the variability of color and fluorescence in low-molecular-weight glass. *Mater. Horiz.* **11**, 5641–5649 (2024).
45. Zhang, J. et al. Exciton Dissociation and Recombination Afford Narrowband Organic Afterglow Through Efficient FRET. *Adv. Mater.* **36**, e2404769 (2024).
46. Dai, W. et al. Excited-State Modulation of Aggregation-Induced Emission Molecules for High-Efficiency Triplet Exciton Generation. *ACS Mater. Lett.* **3**, 1767–1777 (2021).
47. Liang, Y. et al. Enabling Highly Robust Full-Color Ultralong Room-Temperature Phosphorescence and Stable White Organic Afterglow from Polycyclic Aromatic Hydrocarbons. *Angew. Chem. Int. Ed.* **63**, e202318516 (2024).
48. Zhang, J. et al. Highly Efficient and Robust Full-color Organic Afterglow through 2D Superlattices Embedment. *Adv. Mater.* **34**, e2206712 (2022).
49. Cao, S., Fan, W., Chang, R., Yuan, C. & Yan, X. Metal Ion-Coordinated Biomolecular Noncovalent Glass with Ceramic-like Mechanics. *CCS Chem.* **6**, 2814–2824 (2024).
50. Zheng, W.-F., Chen, J., Qi, X. & Huang, Z. Modular and diverse synthesis of amino acids via asymmetric decarboxylative protonation of aminomalonic acids. *Nat. Chem.* **15**, 1672–1682 (2023).
51. Lu, T. Visualization Analysis of Covalent and Noncovalent Interactions in Real Space. *Angew. Chem. Int. Ed.* **64**, e202504895 (2025).
52. Wang, Y. et al. Host-guest doped room/high-temperature phosphorescence of diarylfuro[3,2-b]pyridine derivatives. *Chem. Eng. J.* **489**, 150919 (2024).
53. Tang S., et al. Tandem restriction between spatial confinement and dipole interaction for suppressing thermal quenching of phosphorescence from cycloolefin polymers. *Adv. Mater.* **38**, e14446 (2025).
54. Wang, M. et al. Building a highly stable red/near infrared afterglow library with highly branched structures. *Adv. Mater.* **37**, e2415446 (2025).
55. Qian, Y. et al. Bio-based thermoplastic room temperature phosphorescent materials with closed-loop recyclability. *Adv. Sci.* **12**, e2414439 (2025).
56. Lu, T. & Chen, Q. Independent gradient model based on Hirshfeld partition: a new method for visual study of interactions in chemical systems. *J. Comput. Chem.* **43**, 539–555 (2022).
57. Lu, T. & Chen, F. Multiwfn: a multifunctional wavefunction analyzer. *J. Comput. Chem.* **33**, 580–592 (2012).
58. Humphrey, W., Dalke, A. & Schulten, K. VMD: visual molecular dynamics. *J. Mol. Graph.* **14**, 33–38 (1996).

Acknowledgements

This work was supported by the financial support from the National Natural Science Foundation of China (22405194), the Master's Innovation Foundation of Wenzhou University (3162024003049), the Scientific Research Innovation Capability Support Project for Young Faculty (ZYGXQNJSKYCXNLZCXM-M3), and the National Key R&D Program of China (Grant No. 2024YFA1211600).

Author contributions

W.D., Y.L., X.H., and D.Y. designed the research work and revised the manuscript. C.C. synthesized and prepared the materials. C.C. and L.Z. carried out photophysical property measurements. Y.Y. carried out theory calculations. W.D. and C.C. wrote the manuscript. Y.L., M.L., H.W., X.H., and D.Y. edited the manuscript. All authors discussed the results and commented on the manuscript.

Competing interests

The authors declare no competing interests.

Additional information

Supplementary information The online version contains supplementary material available at https://doi.org/10.1038/s41467-026-68590-2.

Correspondence and requests for materials should be addressed to Wenbo Dai, Yunxiang Lei, Xiaobo Huang or Dongpeng Yan.

Peer review information *Nature Communications* thanks the anonymous reviewers for their contribution to the peer review of this work. A peer review file is available.

[1]School of Chemistry and Materials Engineering, Wenzhou University, Wenzhou, China. [2]School of Environment and Safety Engineering, North University of China, Taiyuan, Shanxi, China. [3]Shaanxi Qinghua Vehicle Safety Systems CO., LTD, Xi'an, Shaanxi, China. [4]Key Lab of Biohealth Materials and Chemistry of Wenzhou, Wenzhou, China. [5]Beijing Key Laboratory of Energy Conversion and Storage Materials, Key Laboratory of Radiopharmaceuticals of Ministry of Education, College of Chemistry, Beijing Normal University, Beijing, China. [6]These authors contributed equally: Chuanli Chen, Yuezhen Yang.
✉e-mail: wbdai@wzu.edu.cn; yunxianglei@wzu.edu.cn; xiaobhuang@wzu.edu.cn; yandp@bnu.edu.cn